Supporting Information for:

Triplet-Fusion Upconversion Using a Rigid Tetracene Homodimer

Christian J. Imperiale[†], Philippe B. Green[†], Ethan G. Miller[‡], Niels H. Damrauer[‡], Mark W. B. Wilson[†]*

† Lash Miller Chemical Laboratories, University of Toronto, Department of Chemistry, Toronto, Ontario, M5S3H6, Canada

‡ University of Colorado, Boulder, Department of Chemistry and Biochemistry, Boulder, Colorado, 80302, United States

*E-mail: mark.w.b.wilson@utoronto.ca

Materials

Palladium(II) 1,4,8,- 11,15,18,22,25-octabutoxyphthalocyanine ($PdPc(OBu)_8$) (Batch #: JB17-11741) and rubrene (sublimed, 99.9%) were obtained from Frontier Scientific and Angstrom Engineering, respectively, and used without further purification. 5,12-Bis((triisopropylsilyl)ethynyl)tetracene (TIPS-Tc) and TIPS-BTc were synthesized as previously reported[1–3]. Spectroscopic grade toluene was obtained from Fisher Scientific.

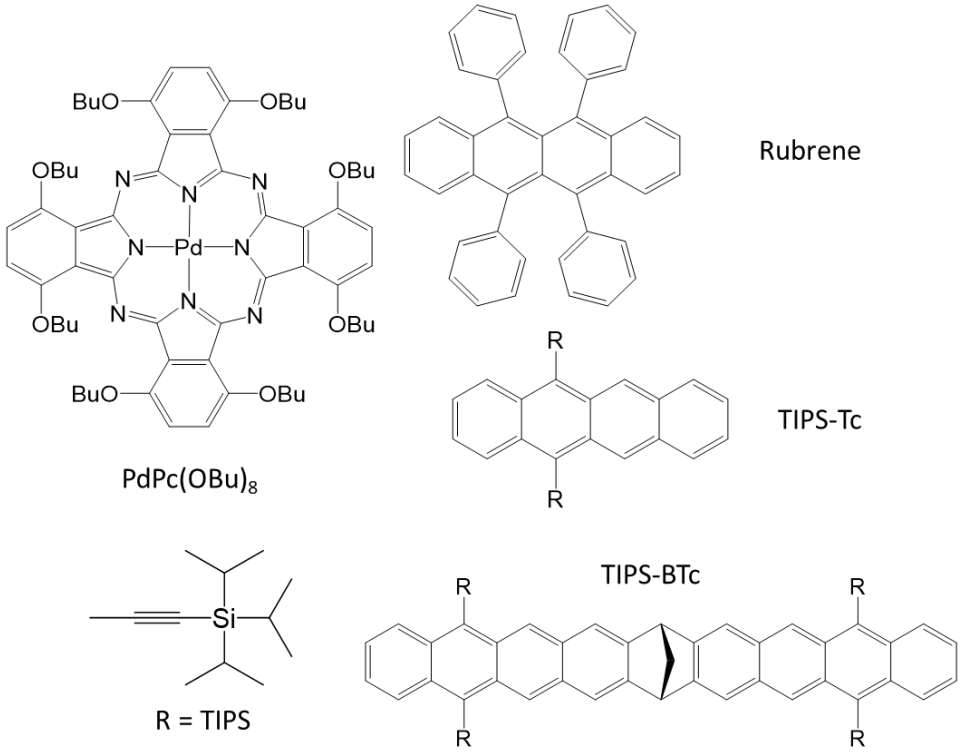

Scheme S1. Molecular chromophores used in this study. $PdPc(OBu)_8$ (palladium(II) 1,4,8,-11,15,18,22,25-octabutoxyphthalacyanine) acts as the triplet sensitizer, while triisopropylsilane-functionalized bistetracene (TIPS-BTc), TIPS-Tc, and rubrene act as the annihilators.

Spectroscopy Experiments

All spectra were acquired in deaerated toluene, prepared at < 5 ppm O_2. De-aeration via nitrogen sparging took place for approximately 3 minutes per mL of solvent. Steady-state absorption spectra were acquired with a Lambda 25 UV-Vis spectrometer. Steady-state mission spectra were taken with a home-built set-up at the indicated excitation wavelength. For (UC) excitation at λ: 730 nm, an externally driven (ThorLabs, LDC205C), 40 mW diode (ThorLabs, HL7302MG) was used. For (direct) excitation at λ: 450 nm, a 5 mW diode (ThorLabs, CPS450) was used. The emission set-up used an off-axis parabolic collimating mirror to direct collected fluorescence to an optical fibre-coupler, which was then sent to an Ocean Optics Flame (visible) or NIRQuest spectrometer (infrared).

Time-resolved emission lifetime measurements were acquired using a λ: 470 nm pulsed diode laser (PicoQuant, LDH-D-C-470), and data was collected using a single photon avalanche diode (Excelitas, SPCM-850-64-FC) and PicoQuant HydraHarp 400 event timer.

Photoluminescence quantum yield and UC quantum efficiency measurements were acquired using the same diodes at λ: 450 nm and λ: 730 nm, and emission from samples was collected using an integrating sphere (GigaHertz-Optik UPB-150-ARTA), coupled to a ThorLabs silicon detector (DET36A).

Supplementary Figures:

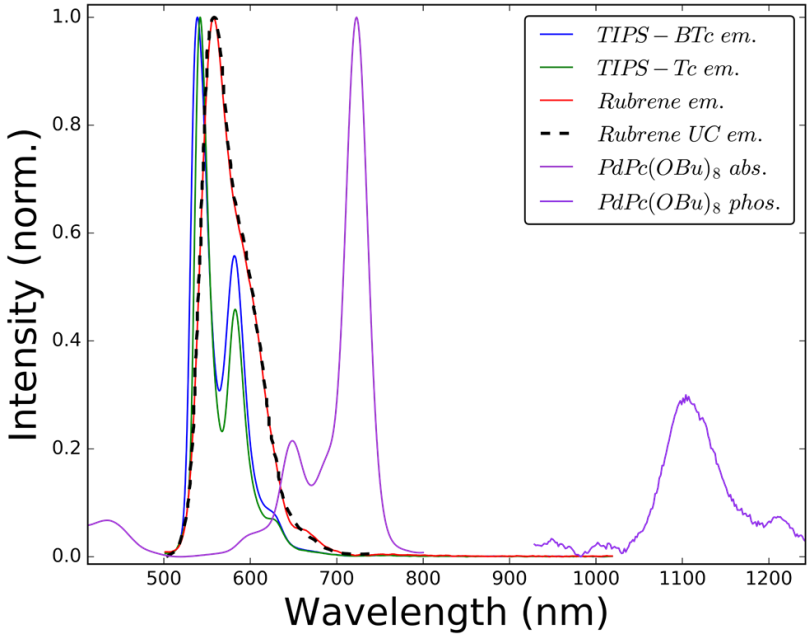

Figure S1. $PdPc(OBu)_8$ steady-state absorption spectrum (purple, normalized to peak) and phosphorescence spectrum (violet, normalized to 0.3 for clarity, excitation at λ: 730 nm, ~20 mW/cm^2). Fluorescence spectra of the three annihilator molecules used in this study (blue, TIPS-BTc; green, TIPC-Tc; red, rubrene), each obtained under steady-state, direct excitation at λ: 450 nm (~2 mW/cm^2).

Table S1. Direct excitation PLQY of TIPS-BTc and TIPS-Tc.

Material	**Measured PLQY**	**Literature PLQY**
TIPS-BTc	0.69 ± 0.05	0.72 ± 0.09 (Ref. 3)
TIPS-Tc	0.72 ± 0.05	0.74 ± 0.08 (Ref. 2)
Rubrene	0.90 ± 0.05	0.98 (Ref. 4)

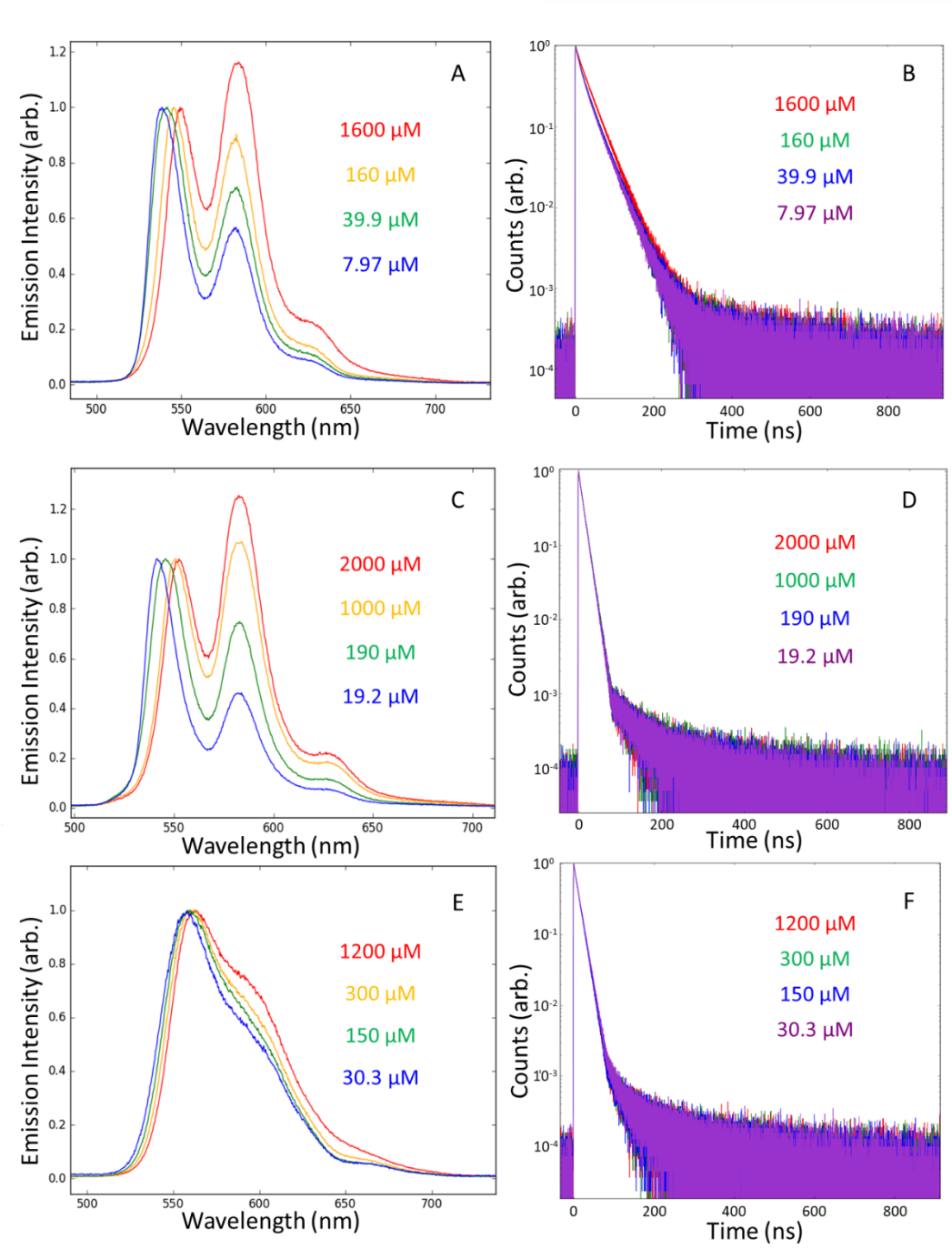

Figure S2. Emission spectra of various solutions of A) TIPS-BTc, C) TIPC-Tc, and E) rubrene under direct excitation at λ=450 nm. Each spectra is normalized to its 0→0 vibronic peak near λ=550 nm. Higher concentrations show evidence of reabsorption, marked by apparent/relative enhancement of features at longer wavelengths.

Photoluminescence (PL) decay dynamics of solutions of B) TIPS-BTc, D) TIPS-Tc, and E) rubrene following direct photoexcitation at λ=470 nm. Traces are background-subtracted (using data from t<0ns), and normalized to the maximum. The very similar decay dynamics are inconsistent with substantial aggregation at these concentrations.

UC Power Dependence

Power dependent UC measurements were obtained by collecting UC emission spectra at various incident excitation powers. A knife-edge measurement of the size of the excitation beam at the sample position allowed for calculation of the incident intensity. The resulting emission spectra were numerically integrated, and the integrated brightness was plotted.

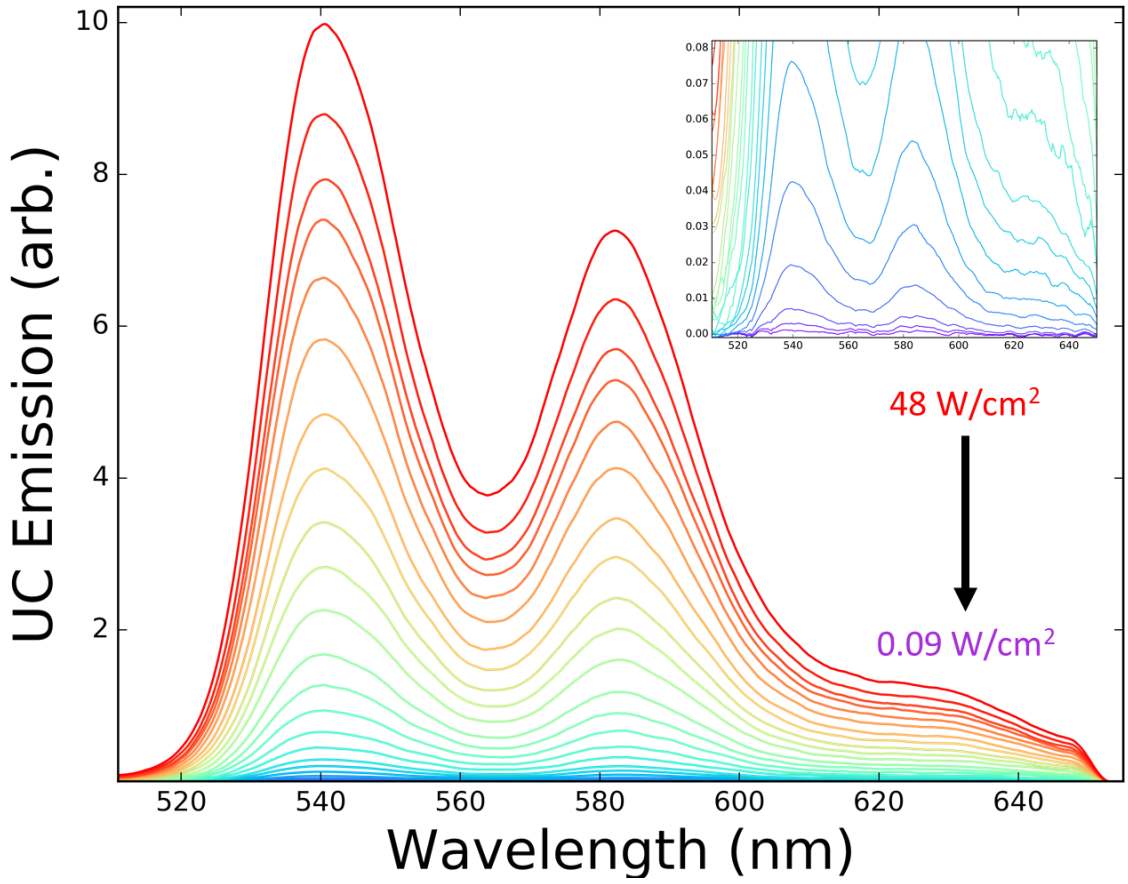

Figure S3. Representative upconversion emission spectra from a power dependent measurement of a solution of $PdPc(OBu)_8$-sensitized TIPS-BTc (0.40 mM; see Figure 1B, green trace). These spectra were collected at 48, 42, 37, 33, 29, 26, 22, 18, 15, 12, 10, 7.5, 6.0, 4.5, 3.5, 2.5, 1.7, 1.4, 1.0, 0.75, 0.50, 0.33, 0.20, 0.13, and 0.09 W/cm^2. Longer integration times were used for low-power measurements. We confirmed that the signal varied linearly with integration time in this regime, so the data could be directly scaled. Incident power was varied allowing for the collection of numerous spectra with various integration times. Inset: zoomed presentation of lowest intensity measurements to show maintenance of curve structure at low laser fluence. Curves such as the final curve here at 0.09W/cm^2 were omitted from power dependence plots (e.g. Fig 2B) due to low signal/noise.

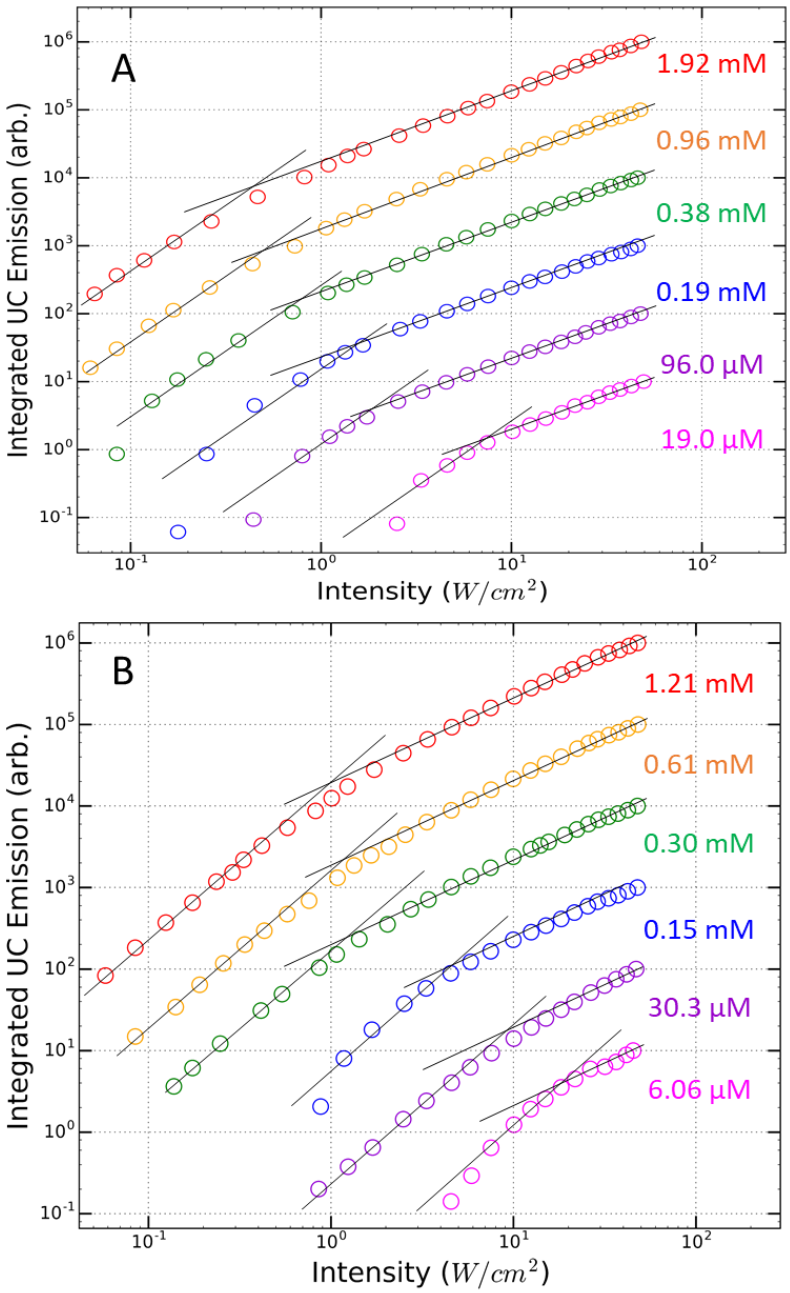

Figure S4. A) Power dependent UC measurements of solutions of PdPc(OBu)$_8$-sensitized (72.5 µM) TUC with A) TIPS-Tc and B) rubrene, with the annihilator at the stated concentrations. These data are summarized in Figure 2A in the main text, along with data from the comparable curves for TIPC-BTc that appear as Figure 1B. The intensity threshold for the onset of the linear regime for UC efficiency in both plots displays the saturable trend discussed in the main text. These data are from the experiment for each annihilator that achieved the lowest threshold for max-efficiency upconversion.

Triplet-Fusion Upconversion Quantum Efficiency (UCQE)

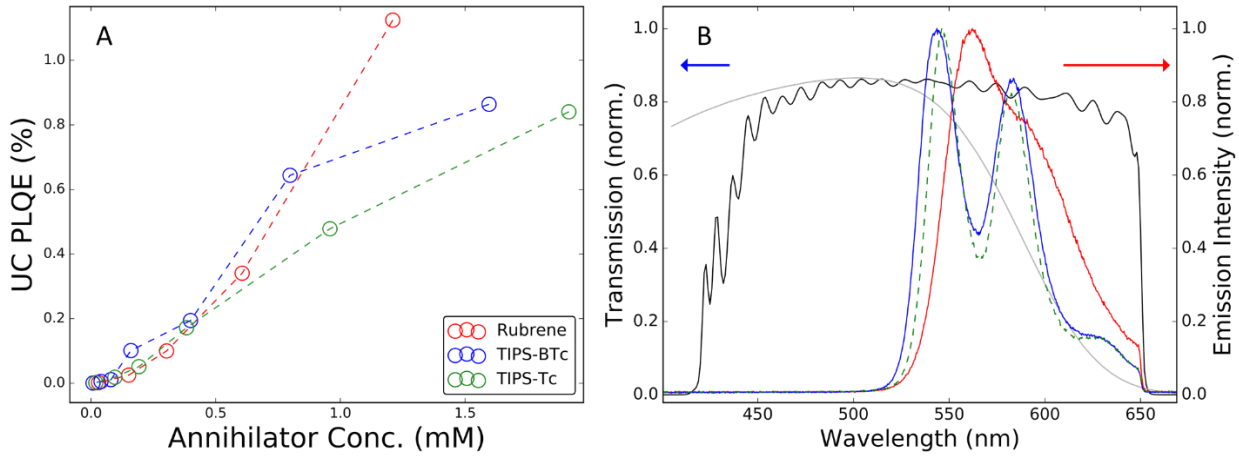

Figure S5. A) Concentration dependence of UCQE. The absolute QY of the UC process was measured under max-efficiency excitation fluence using an integrating sphere. This figure shows that the samples become brighter as the annihilator concentration is increased, consistent with our simulation results (Figure S12). Note that the concentration dependence does not give full information about the ultimate use of sensitized triplet excitons (see Figure 3, main text). UCQE is scaled to the direct excitation PLQY for each annihilator, correcting for the <100% direct excitation PLQY of the annihilators.[5] In this plot, a UC PLQE of 100% would represent a system in which every absorbed photon contributes to upconversion (i.e. 100 low-energy photons enter the system, resulting in 50×PLQY photons emitted at twice the energy, and thus a nominal 100% energy conversion).

B) Left axis: normalized transmission of optical filters used for PLQE studies. The dielectric short-pass filter (black trace; ThorLabs FESH650) was used for all steady-state spectra and direct comparisons of UC emission. The colored glass filter (dark grey trace; ThorLabs FGB39) was used for absolute QY measurements in the integrating sphere to avoid artifacts from wide-angle emission. This difference in filtering caused the absolute PLQE of slightly-redder rubrene in Figure S5A to appear lower than that of TIPS-Tc. In Figure 3A (main text), the dielectric filter is used in order to show the reality of the situation; namely that TIPS-Tc is less bright than rubrene and TIPS-BTc at these comparable concentrations. Right axis: emission spectrum of rubrene (red trace), TIPS-BTc (blue trace), and TIPS-Tc (green dashed trace) showing the amount of emission intensity lost due to optical filtering with the colored glass filter.

Kinetic Simulations

Foundational rate equations:

Building from previously proposed kinetic arguments for triplet fusion[6,7] the rate equation for the concentration of triplet-excited annihilator molecules in solution is:

$$\frac{d[^3A^*]_t}{dt} = -k_{TF}[^3A^*]_t^{\,2} - k_{HF}[^3A^*]_t[^3S^*]_t - k_{Tdec}[^3A^*]_t + k_{TET}[^3S^*]_t[A]_t \qquad \text{(S1)}$$

Where:

- $[^3A^*]_t$ is the concentration of triplet-excited annihilator in solution
- $[A]_t$ is the concentration of ground-state annihilator in solution
- $[A_0] = [^3A^*]_t + [A]_t$ is the total concentration of annihilators in solution, which is independent of time.
- k_{TF} is the bimolecular rate constant for triplet fusion between two annihilators in the excited state resulting in a spin-singlet state.
- k_{HF} is the bimolecular rate constant for triplet heterofusion when an excited-state annihilator directly interacts with an excited-state sensitizer. In a minor extension of the previous model,[6] we explicitly include a channel for heterogeneous fusion so that the model is robust to extremes of excitation intensity and annihilator concentrations. Then, as discussed further below, we assert that $k_{HF} \approx \frac{k_{TET}}{4}$ for the purposes of this analysis.
- k_{Tdec} is the monomolecular rate constant decay of the annihilator in the spin-triplet excited state
- k_{TET} is the rate constant for triplet energy transfer from the sensitizer to the annihilator
- $[^3S^*]_t$ is the concentration of excited-state sensitizer molecules
- $[S]_t$ is the concentration of ground-state sensitizer molecules
- $[S_0] = [^3S^*]_t + [S]_t$ is the total concentration of sensitizers in solution, which is constant. These last three definitions allow us to explicitly account for occupation-bleaching of the sensitizer absorption.

We additionally define four parameters concerning the excitation and photophysics of the sensitizer.

- Φ_{Laser} is the photon flux of the excitation laser
- σ_{sens} is the absorption cross-section of the sensitizer molecules
- η_{isc} is the efficiency of inter-system crossing from the singlet to triplet excited states of the sensitizer
- k_{Phos} is the inverse phosphorescence lifetime of the isolated sensitizer, which includes all radiative and non-radiative monomolecular decay channels

We then set up a rate equation for $[^3S^*]_t$, the concentration of triplet-excited sensitizer molecules in solution, including the effects of laser excitation and absorption bleaching due to state-filling, monomolecular decay, and triplet energy transfer:

$$\frac{d[^3S^*]_t}{dt} = \Phi_{Laser}\left[S_0 - {}^3S^*\right]\sigma_{sens}\eta_{isc} - k_{Phos}[^3S^*]_t - k_{TET}[A_0][^3S^*]_t \qquad \text{(S2)}$$

Discussion of heterofusion:

As stated in the main text, we use of the total annihilator concentration in the final term following our assumption that all interactions between an excited-state sensitizer and an annihilator molecule result in the de-excitation of the sensitizer with the same rate constant. This is motivated by the similar numeric values of experimentally-determined co-efficients for homofusion and TET (Table S8, noting the expected effect of molecular size on diffusivity), and from the expectation that the overall rate will be dominated by the timescale of diffusion, because exciton transfer/exciton-exciton interactions and thermalization are fast by comparison.

We note that we cannot rule out a 'harpoon'-like effect, where the favourable energetics of the dimer-sensitizer interaction complex provide an attractive potential that could accelerate heterofusion relative to triplet energy transfer. Although we would not expect this to overcome Brownian diffusion at room temperature, we note that the stabilization of a favourable interaction complex in a sterically-congested energy landscape was proposed for diffusion-mediated fission in TIPS-pentacene.[8] However, our present data set does not meaningfully test this hypothesis, so we do not discuss this further except to note that even a 40-fold relative enhancement of HF over TET is insufficient to reproduce our experimental observations for the dimer. (See Figure S10)

Explicitly, as shown in Equation S3, we would consider the two de-excitation channels for the excited sensitizer, either TET to a ground-state annihilator, or triplet transfer/fusion with an excited-state annihilator.

$$k_{TET}[A_0][^3S^*]_t = k_{TET}[\,{}^3A^*]_t[^3S^*]_t + k_{TET}[A]_t[^3S^*]_t \qquad \text{(S3)}$$

Then, in comparing the rate of sensitizer quenching due heterofusion in S3 (*i.e.* $k_{TET}[\,{}^3A^*]_t[^3S^*]_t$), with the rate of depleting triplet-excited annihilators via heterofusion in S1 (*i.e.* $k_{HF}\left[\,{}^3A^*\right]_t[^3S^*]_t$), the spin statistical factors for simplest model (cf. below) for fusion of uncorrelated triplets would require that: $k_{TET}[\,{}^3A^*]_t[^3S^*]_t = 4k_{HF}[^3A^*]_t[^3S^*]_t$ This is because for every 'productive' transfer that generates a spin-singlet triplet-pair, leading to photon emission and depletion of the triplet-excited annihilator, there would be three 'unproductive' sensitizer-depleting transfers that generate a triplet-pair state in the triplet manifold (${}^3TT$). We assume that these states rapidly thermalize to single triplet excitation, leaving the concentration of triplet-excited annihilators unchanged. With these assumptions, we replace $k_{HF} = \frac{k_{TET}}{4}$ in S3:

$$k_{TET}[A_0][^3S^*]_t = 4k_{HF}[\,{}^3A^*][^3S^*]_t + k_{TET}[A][^3S^*]_t \qquad \text{(S4)}$$

Thus, the simplified form at left follows direction from our assertion that $k_{HF} = \frac{k_{TET}}{4}$.

These assertions reflect a generous view of heterofusion, as there are photophysical arguments for why heterofusion might not efficiently generate upconverted emission. Particularly, unlike homofusion, the bimolecular ^1TT state generated in heterofusion might relax not only to the lowest-energy spin-singlet exciton on the annihilator ($^1A^*$: leading to the desired upconverted emission), but also to the lowest-energy singlet excitation of the sensitizer ($^1S^*$) so that the annihilator is effectively de-excited without photon generation. Many kinetic factors would influence the efficiency of this process, including the nature/duration of the interaction complex, and the coupling between molecular states. For instance, our annihilators and sensitizer (as is common in the triplet fusion community[9]) have poor spectral overlap for FRET (Figure S1), but this channel might still contribute. Still, the lowest-energy spin-singlet excitation on $PdPc(OBu)_8$ is $\gtrsim$0.5 eV below the relaxed $^1A^*$, so a majority of the population would be transferred if local equilibrium were reached.

We then considered the consequences to our model if heterofusion was inefficient in this way. Firstly, the primary effect would be to reduce the fraction of emission generated via the heterofusion term described in Equation S9. By contrast, there would be no direct change to the excited-state annihilator population (Equation S1), as our model already considered that every heterofusion interaction yielding an overall spin-singlet state depleted the annihilator. However, there would be an indirect increase in the excited-state sensitizer population, all else equal, as the sensitizer would not be ultimately de-excited in any 'unproductive' heterofusion interaction. This would cause the term in Equation S2 $k_{TET}[A_0][^3S^*]_t$ to be replaced by $k_{TET}[A][^3S^*]_t$ (where$[A]$ is the concentration of annihilators in the ground state only), so the relative contribution of this term would be slightly smaller at steady state.

Thus, we consider that inefficient heterofusion would only significantly alter the simulated steady-state populations in experimental regimes where an appreciable fraction of the annihilators are excited, which is identically the criteria for experimental conditions under which heterofusion with our standard assumptions is appreciable (Figure S8,S10). As we describe in the main text, and discuss further below, these conditions are not those where TUC is efficient.

Thus our assumptions reflect a heterofusion that would have the greatest plausible impact on the overall photophysics of this system, and our model shows that this effect is small, and results in a distinct functional form from the anomalous concentration-dependence of the threshold observed for the dimer. As we discuss in the main text, we do not consider that heterofusion is the reason for the unusual photophysics of the rigid dimeric annihilator, and we consider that any 'inefficiency' of heterofusion would only strengthen this argument.

Comment on triplet-pair states in the quintet manifold:

In our present model, we follow convention[10,11] and do not explicitly consider triplet-pair states in the overall-quintet manifold (i.e. ^5TT), despite the expectation that an interaction complex of two triplet-excited annihilators would naively be expected to generate this state frequently (5/9th of encounters viewed conventionally,[9–11] 5/16th of encounters per. Scholes[12]) This is because

while a bimolecular ^1TT state can populate the roughly isoergic molecular singlet exciton (which rapidly emits), and a bimolecular ^3TT state can rapidly relax to a low-energy molecular triplet exciton via internal conversion, it is not expected that monomers have a energetically-accessible four-electron overall-quintet state.[11] Thus, because other relaxation channels for the ^5TT state are spin-forbidden and slow, there is a preference for overall-quintet interaction complexes to ultimately re-dissociate to free triplets.[11] Similar arguments apply to the role of ^5TT in heterofusion with monomeric annihilators.

However, further to our discussion in the main text, we speculate on the possible role that ^5TT states might play in the unexplained discrepancy between the concentration-dependent threshold of the dimer and the standard kinetic model developed here. In sharp contrast to monomeric annihilators, ^5TT states are expected to be thermodynamically accessible at room temperature in this class of weakly-coupled dimers,[3,13] and thus could be generated via bi-molecular interactions. Even so, we note that our model and assertions would equally describe the behaviour of dimeric annihilators in the limit where spin-dephasing either 1) is slow compared to the characteristic time of diffusional interactions or 2) populates all nine triplet-pair states equally. We consider each case.

1) In the straightforward first case, very long-lived dimeric ^5TT states would tend to re-dissociate to individual triplets through subsequent collisions with other annihilator molecules. As a result, interactions forming ^5TT states would have little ultimate effect on the steady-state excited-state populations.
2) The second case echoes our fundamental assumption that the overall rate of interactions will be effectively diffusion-controlled. Here, if dephasing (i.e. loss of spin correlation) between the triplet-pair spin-multiplicities were rapid and equally-distributed, any dimeric ^5TT state formed would ultimately generate a triplet-pair state in the singlet manifold ($i.e.$ ^1TT), or triplet manifold (^3TT) with the same 1:3 probability as two uncorrelated triplets.[9,10] As before, we expect that ^1TT states would rapidly couple to emissive singlet excitons, and ^3TT states would thermalize to a single spin-triplet excitation.[14,15] Thus, under these conditions, the inclusion of ^5TT states in the model would not change the functional form of the inverse-threshold-vs-annihilator concentration curve, as it would only affect the value of the overall scaling η_f between the rate of molecular interactions and photon emission.

However, as we describe in the main text, an intriguing speculative case builds on spectroscopic and spin-resonance studies of analogous molecules where singlet exciton fission is preferred,[3,15,16] where it is noted that symmetry conditions render zero-field coupling stronger between the ^5TT and ^1TT states, than the (spatially anti-symmetric) ^3TT.[15–17] However, this is a topic of ongoing research: experiments on a terylene dimer have instead showed stronger coupling between the triplet and quintet manifolds,[14] and calculations have shown a strong dependence of the coupling on molecular orientation.[18]

However, if the possibility that ^5TT states on the dimer preferentially generate ^1TT states (rather than ^3TT) were directly extensible to our rigid dimer at room-temperature, the effect would be to introduce a concentration-dependence to the spin-statistical factor for triplet fusion. At high concentrations, where collisions were more rapid than spin dephasing, this would revert to Case 1) above, and spin-dephasing would have no net effect. However, at sufficiently low concentrations, we would expect a boost in the overall emission relative to a monomeric control, because (depending on the selectivity of intra-manifold dephasing) up to ~6/9^{ths} of triplet-triplet encounters (homo- or hetero-fusion) could ultimately lead to singlet generation and emission, rather than the conventional 1/4 factor used for monomers.

An extrapolation from the diffusion constant of a similarly TIPS-functionalized acene[8] suggests that average time between homo-annihilator-collisions at our highest experimental concentrations is on the order of the spin-dephasing time previously observed for crystalline tetracene,[19] and that dephasing would be more rapid than collisions at lower concentrations. For this reason, we consider this possibility an intriguing area for further study, though the ability for fusion-based experiments to discriminate between mechanisms is limited due to the convolution of many kinetic processes. By contrast, kinetic studies of the reverse process, singlet exciton fission, in these systems may continue to provide meaningful insight.[8,14–16,19]

Functional form of the intensity- and concentration-dependent upconverted emission:

Returning to the development of the model, Equation S2 is taken to the steady-state limit to give an expression for $[^3S^*]_t$ in terms of experimental parameters and literature values:

$$[^3S^*]_t = \frac{\Phi_{Laser}[S_0]\sigma_{sens}\eta_{isc}}{k_{Phos}+k_{TET}[A_0]+\Phi_{Laser}\sigma_{sens}\eta_{isc}} \qquad \text{(S5)}$$

Equation S1 itself is taken to the steady state limit to determine $[^3A^*]_t$, the concentration of triplet-excited annihilator in solution.

$$0 = -k_{TF}[^3A^*]^2 - \frac{k_{TET}}{4}[^3A^*][^3S^*] - k_{Tdec}[^3A^*] + k_{TET}[^3S^*]([A_0] - [^3A^*]) \qquad \text{(S6)}$$

$$0 = -k_{TF}[^3A^*]^2 - \left(k_{Tdec} + \frac{5}{4}k_{TET}[^3S^*]\right)[^3A^*] + k_{TET}[^3S^*][A_0] \qquad \text{(S7)}$$

This can be solved using the quadratic equation to give an expression for the steady-state concentration of triplet-excited annihilators:

$$[^3A^*] = \frac{\left(k_{Tdec}+\frac{5}{4}k_{TET}[^3S^*]\right) \pm \sqrt{\left(k_{Tdec}+\frac{5}{4}k_{TET}[^3S^*]\right)^2 - 4(-k_{TF})(k_{TET}[^3S^*][A_0])}}{2(-k_{TF})} \text{(S8)}$$

Into which we can substitute the expression for $[^3S^*]$ from Equation S5.

When considering a range of annihilator concentrations and laser fluxes, this expression returns one set of real solutions and a set of inadmissible solutions (negative concentrations), the latter of which are disregarded.

Then, the steady-state brightness of upconverted fluorescence can be described by:

$$N_f = \eta\left(k_{TF}[^3A^*]^2 + \frac{1}{4}k_{TET}[^3A^*][^3S^*]\right) \qquad \text{(S9)}$$

Where the first term represents the traditional triplet fusion between two excited-state annihilators, and the second term represents photon emission following heterofusion—triplet fusion between an excited-state annihilator and an excited-state sensitizer. This latter term is often small for high-efficiency upconversion (when sufficient annihilator is available to quench the sensitizer, or when long-lived annihilator triplets allow a large concentration to build up) but contributes at some experimentally-achievable cases modelled below. As discussed above, we consider that this is the maximum plausible contribution of heterofusion, and the second term would be reduced by a multiplicative factor if interactions between $^3S^*$- $^3A^*$ with overall-singlet spin generate annihilator emission less efficiently than standard homofusion ($^3A^*$- $^3A^*$). Lastly, , η is a proportionality constant encompassing direct excitation PLQY and spin-statistical factors.

Conceptual validation of kinetic simulations

Note: All figures generated using the kinetic model described by equations S5, S8, and S9 (i.e. including heterofusion) except where explicitly stated.

Table S2. Kinetic parameters for Figures S6-S8.

	All curves
k_{TF} (M^{-1} s^{-1})	7.14×10^{7}
k_{TET} (M^{-1} s^{-1})	3.54×10^{8}
τ_{dec} (s)	2.75×10^{-4}

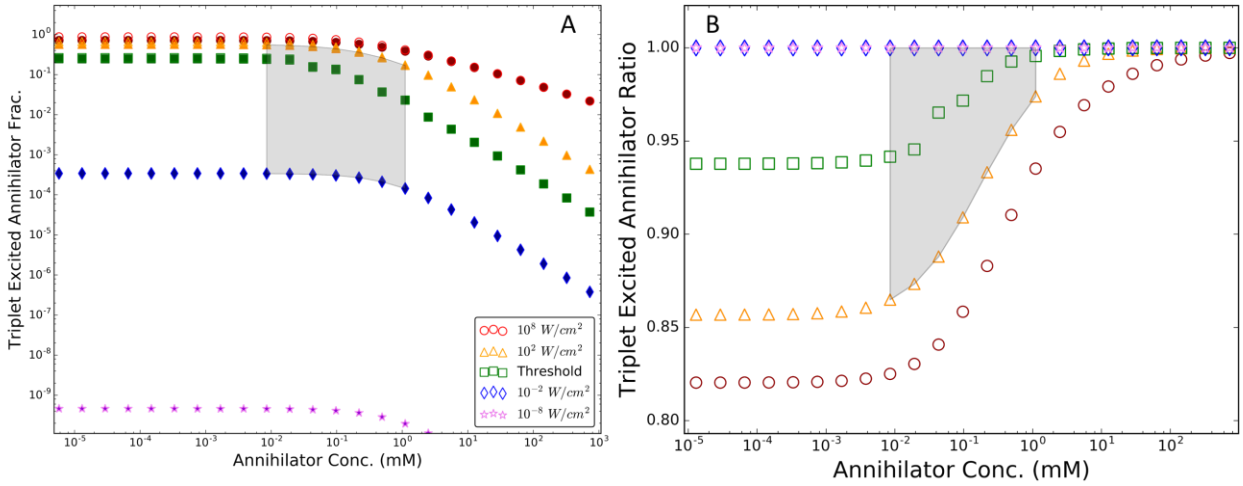

Figure S6. A) Fraction of annihilators in the triplet-excited state as a function of total annihilator concentration (i.e. $[\,^3A^*]$ / $[A]$), with each curve presenting simulated results for rubrene under a specific excitation intensity. (Red circles/violet stars, maximum/minimum simulated excitation intensity; yellow triangles/blue diamonds, maximum/minimum experimental excitation intensity; green squares, excitation at the threshold intensity for max-efficiency upconversion.) The shaded region indicates the range of annihilator concentrations and excitation intensities studied experimentally. A filled marker with a darker shade of each colour indicates the results from simulations including heterofusion, using our assertion that $k_{HF} = \frac{k_{TET}}{4}$.

For a given excitation intensity, the fractional occupation asymptotes to a finite value at low total annihilator concentrations. This is because for sufficiently small $[A]$, $[\,^3A^*]^2$-dependent triplet-triplet recombination will be inefficient, and the steady-state excited-state sensitizer concentration will be governed by monomolecular phosphorescent decay, so that $[S^*]$is a fixed value set by the excitation intensity, absorption cross-section, and the rate constant for monomolecular phosphorescent decay. In this case, the linear $[A]$-depedencies of triplet supply (via $[A]$-dependent TET) and triplet demand (via monomolecular annihilator triplet decay and/or heterofusion), will come into balance. For a given $[A]$, this fraction approaches unity asymptotically at high excitation intensities (*e.g.* yellow and red curves), due to saturation of the

TET channel when most annihilators are excited, causing bleaching of the sensitizer absorption when most sensitizers are occupied.

At high total annihilator concentrations, the modelling predicts a linear decrease of the fraction of triplet-excited annihilators with added annihilators. This is because, for a particular material system, linear-regime upconversion requires a certain absolute concentration of *excited-state* annihilators. As a result, the *fraction* of excited-state annihilators will scale inversely with their total concentration. The roll-over from the low- to high-annihilator concentration regimes represents the competition between these processes with the concentration-dependent TET from the sensitizer.

Lastly, the curves in A) demonstrate that our inclusion of heterofusion does not significantly affect the results of the model. This is illustrated more clearly in B), which plots $\left[{}^3A^*\right]_{hetero}/\left[{}^3A^*\right]_{no\ hetero}$ to capture the relative effect of including heterofusion in the model. We observe that the perturbation of the steady-state concentrations is small for all modelled conditions. The greatest effect under our experimental conditions is a 14% reduction in the fraction of triplet-excited annihilators at our lowest annihilator concentration, under maximum-intensity excitation, where overall upconversion efficiency is low. (See also Figure S8 and S10 for further discussion of the effect of heterofusion.)

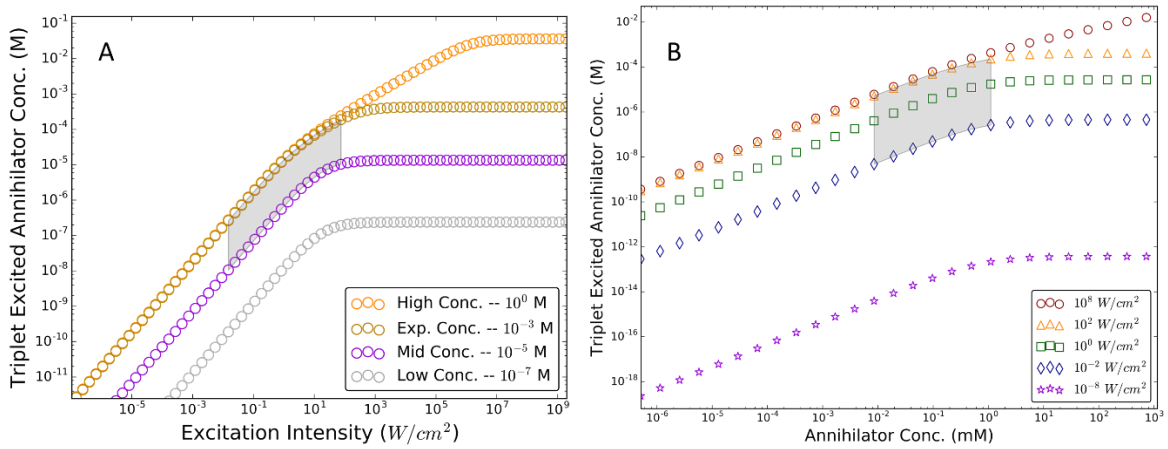

Figure S7. A) Simulated absolute triplet-excited annihilator population as a function of excitation intensity. Note that the curves for the highest simulated concentration (yellow-orange, not experimentally realizable due to solubility) and a typical experimental concentration (dark yellow, 1 mM) directly overlap at low excitation intensities. We observe that the max-efficiency regime (where the UC PL varies linearly with excitation, and $[^3A^*] \propto \sqrt{\Phi_{Laser}}$) starts at a fixed value of $[^3A^*]$ that depends primarily on k_{TF}. If the annihilator concentration is too low to extract a sufficient flux of triplets from the sensitizer, this threshold is never reached. At intensities lower than the threshold for a particular concentration, $[^3A^*] \propto \Phi_{Laser}$ as decay is predominantly monomolecular. $[^3A^*]$ reaches a plateau at the highest excitation fluxes due to saturation of TET, leading to bleaching of the sensitizer absorption due to state-filling.

B) Simulated absolute triplet-excited annihilator population as a function of ground-state annihilator concentration. In the low-concentration limit, the triplet flux from the sensitizer varies linearly with the concentration of the quenching annihilators, and recombination is predominantly monomolecular, so $[^3A^*]$ varies linearly with $[A]$ at all fluences. At higher concentrations, the relationship is more complex, due to the competing effects of monomolecular/bimolecular recombination channels, TET from the sensitizer, and bleaching of the sensitizer absorption. At experimental fluences, $[^3A^*]$ saturates once there are sufficient ground-state annihilators to quantitatively extract triplets from the sensitizer.

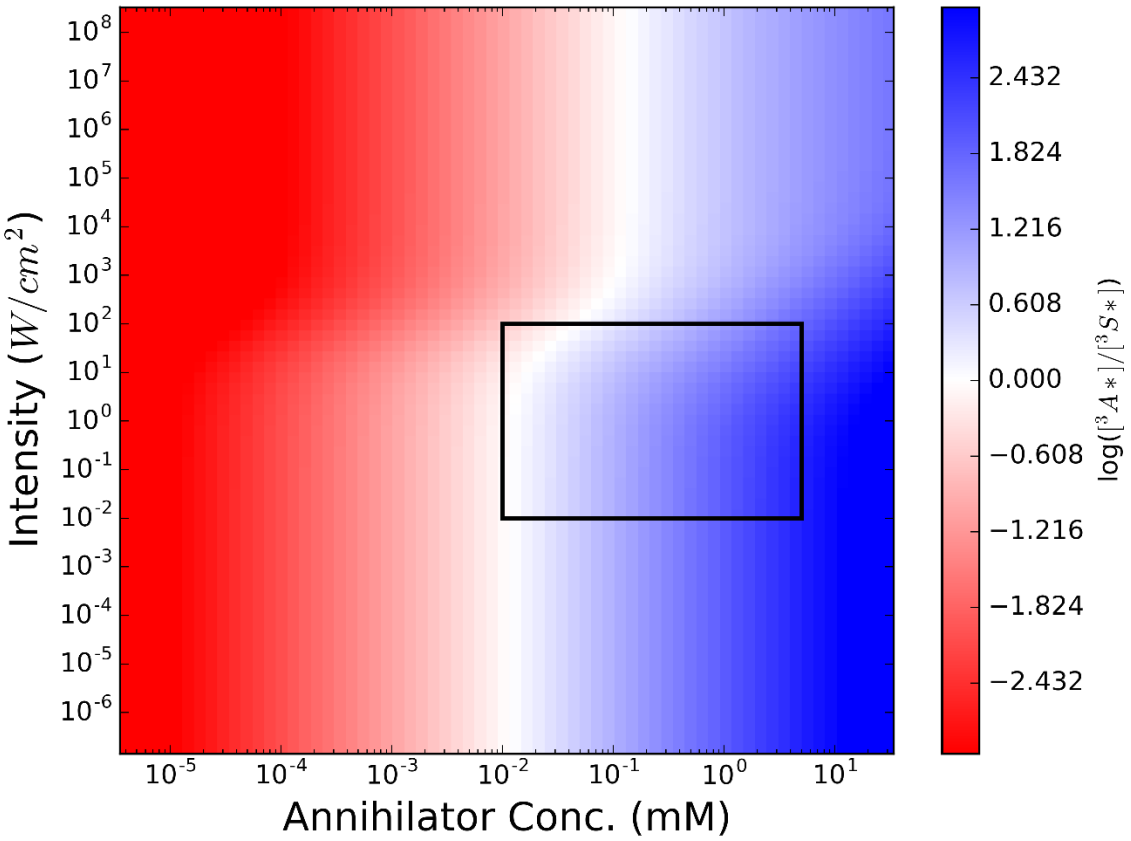

Figure S8. Analysis of heterofusion pathway using the kinetic model, showing the calculated relative concentrations of triplet-excited annihilators to triplet-excited sensitizers over a wide range of ground-state annihilator concentrations and incident intensities. The solid black box indicates the experimental conditions in this work and the blue shades in the logarithmic color map indicate conditions where homofusion interactions would dominate if the rate constants of homo- and heterofusion were equal (Equation S9), a situation comparable to our findings (Table S8). With these assumptions, heterofusion would be expected to generate ~80% of emitted photons (the red region in the top-left corner of the black box), but only with high-intensity excitation at the very lowest experimental annihilator concentrations, where overall upconversion efficiency is low.

Results of Kinetic Simulations: Concentration dependence of max-efficiency threshold

Motivation: Taken together, these simulations (S8–11) show that the threshold for max-efficiency upconversion will saturate for a sufficiently high annihilator concentration, given sufficient excitation fluence, and in the absence of higher-order effects (e.g. quenching processes $\propto [^3S^*]_t$ & $\propto [^1A^*]_t^2$). However, annihilators with a greater k_{TET} will achieve this asymptotic performance at lower concentrations, all things equal. While other parameters (greater τ_{Tdec}, greater k_{TF}) will lower the absolute value of this threshold, and improve absolute performance, it is only k_{TET} that influences the concentration of annihilators required to reach max-efficiency performance.

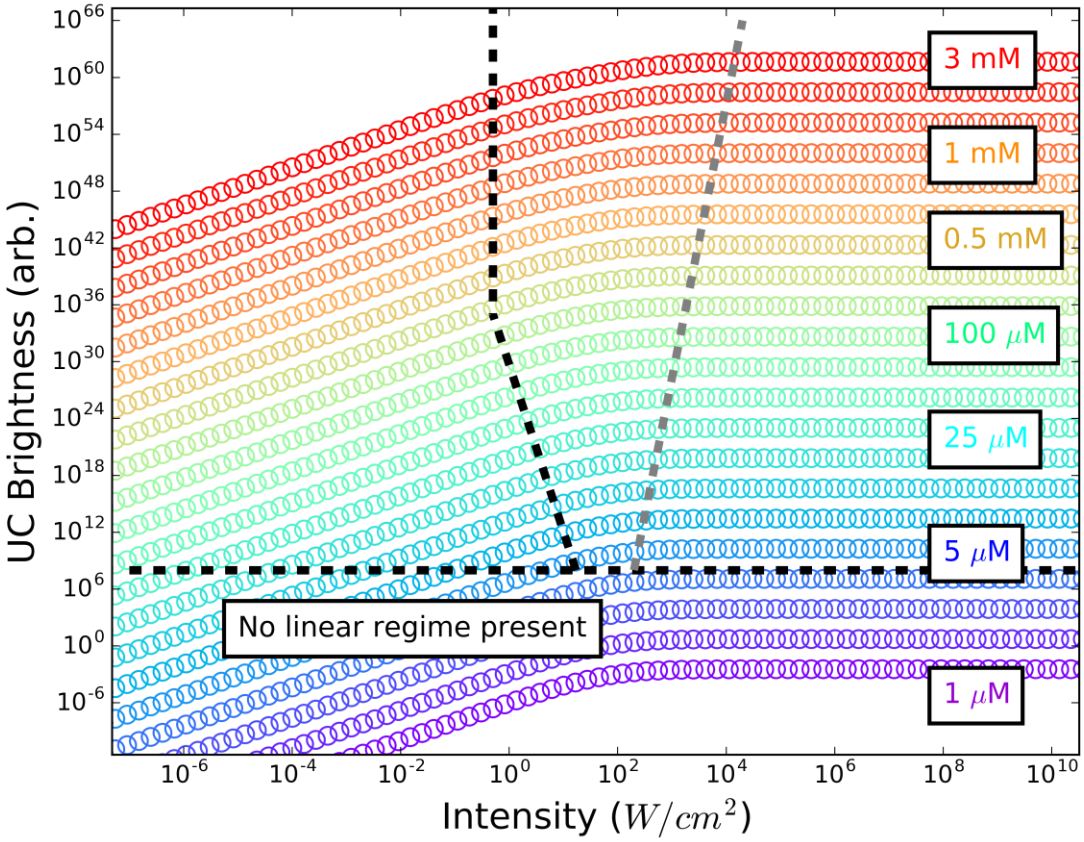

Figure S9. Simulated intensity dependence of UC emission across a range concentrations. The specific parameters used are for rubrene (Table S3). All simulations are calculated with 72.5 µM of PdPc(OBu)$_8$ sensitizer with an absorption cross-section of σ = 2.77x10^{-18} cm^2 (calculated from measured molar absorptivity) and a triplet generation yield of $\eta_{isc} = 75\%$ (a lower bound given the reported phosphorescence quantum yield of PdPc(OBu)$_8$.[20]) The vertical dashed black curve indicates the intensity threshold for the onset of max-efficiency upconversion. Not all annihilator concentrations can achieve linear-regime upconversion. For curves below the horizontal dashed

black line, monomolecular decay of the excited annihilator is dominant for any excitation intensity. However, the brightness of upconverted emission still saturates at high intensities (indicated by the dashed grey line) in these experiments, due to bleaching of the sensitizer absorption, when low concentrations of ground-state annihilators are unable to extract further triplet excitons to continue improving UC. The threshold of the simulated data was determined by fitting lines of slope=1 and slope =2 to each region and determining the intercept.[6]

Table S3. Kinetic parameters for Figure S9.

	Rubrene
k_{TF} (M^{-1} s^{-1})	7.14×10^{7}
k_{TET} (M^{-1} s^{-1})	3.54×10^{8}
τ_{Tdec} (s)	2.75×10^{-4}

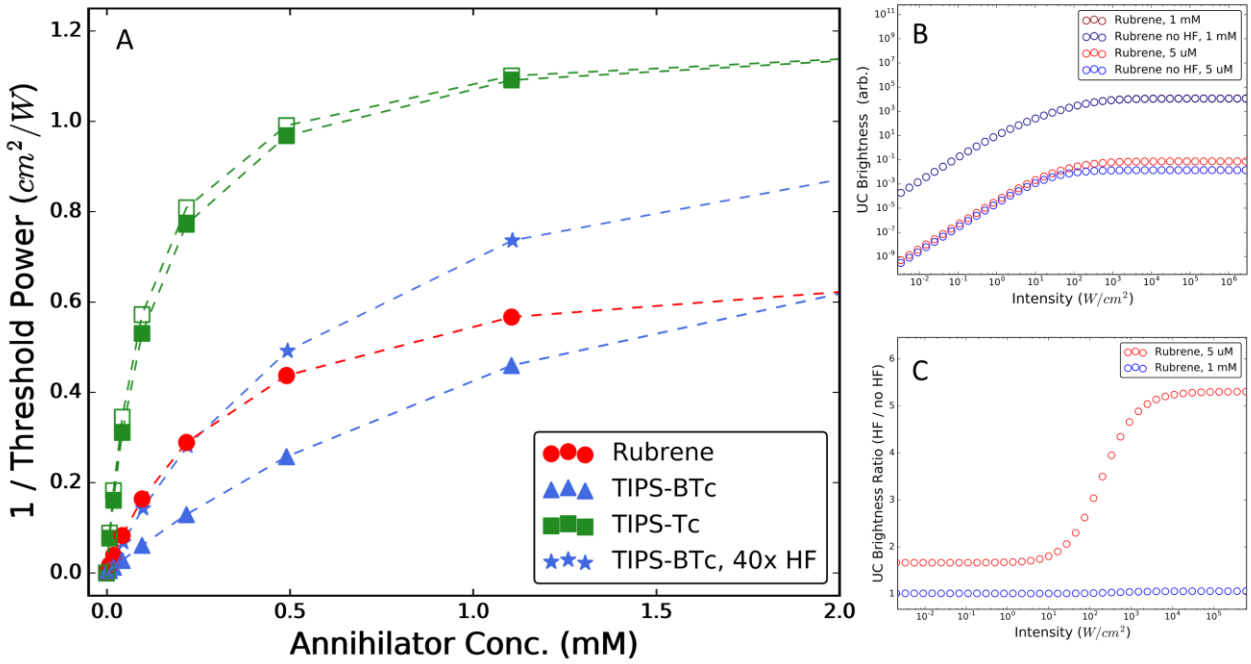

Figure S10. Effect of heterofusion on kinetic model. A) Simulated intensity threshold as a function of ground-state annihilator concentration in solution for the three molecular systems while including (filled points)/excluding (empty points) the heterofusion channel as described above. For the TIPS-BTc and rubrene curves, these data sets are nearly overlaid. Thus, if the rate constant for heterofusion is approximately one-quarter the rate constant for TET, this channel has little effect on the concentration-dependence of the threshold for max-efficiency performance, and does not explain the unusual performance of the dimer.

B,C) Effect of heterofusion on the predicted intensity- and concentration-dependence of the upconversion brightness. Panel B) displays the brightness (arb. units) for rubrene at the highest or lowest experimental annihilator concentrations with and without the inclusion of heterofusion in the model, while panel C) shows the ratio of the curves in B). At high concentrations (B, upper curves; C, lower curve), heterofusion neither has a significant effect on the brightness nor the threshold for max-efficiency performance. At the lowest concentrations (B, lower curves; C upper curve), the inclusion of heterofusion has greater effect on the emission brightness (~1.5-fold increase at excitation intensities below 10 W/cm^2, and 5-fold increase above 1 kW/cm^2.) However, the effect on the threshold is minimal (<1%) for rubrene (red circles). For materials with higher rate constants of TET (i.e. TIPS-Tc, green squares), the inclusion of HF marginally increases the threshold at low concentrations (5% decrease on the above plot, A) but has a negligible effect at higher concentrations (<1% above 1mM). Using the measured k_{TET} of the dimer, we find heterofusion has little effect on the shape of the threshold-vs-annihilator concentration curve for all $k_{HF} < 40 \cdot \left(\frac{1}{4}\right) k_{TET}$. (Starred blue symbols in Figure A)

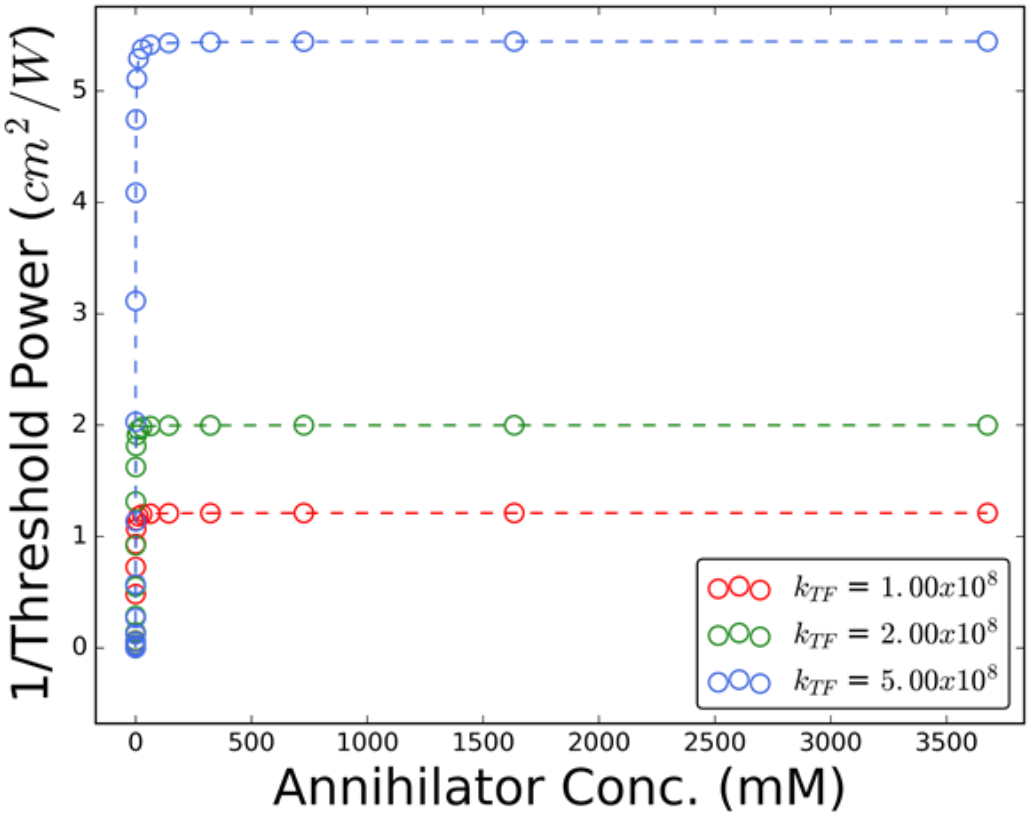

Figure S11. Simulated intensity threshold as a function of ground state annihilator concentration in solution showing the dependence of the threshold intensity on k_{TF}, the rate constant for triplet fusion. The overall rate of bimolecular TF strongly depends on the annihilator concentration, as it requires the diffusion of both triplet-excited annihilators. Thus, annihilators with a higher k_{TF} achieve max-efficiency upconversion at a considerably lower threshold excitation intensity. However, the best-achievable threshold is reached at comparable annihilator concentrations.

Table S4. Kinetic parameters for Figure S11.

	Red	Green	Blue
k_{TF} (M^{-1} s^{-1})	1.00×10^8	2.00×10^8	5.00×10^8
k_{TET} (M^{-1} s^{-1})	1.00×10^8	1.00×10^8	1.00×10^8
τ_{Tdec} (s)	2.75×10^{-4}	2.75×10^{-4}	2.75×10^{-4}

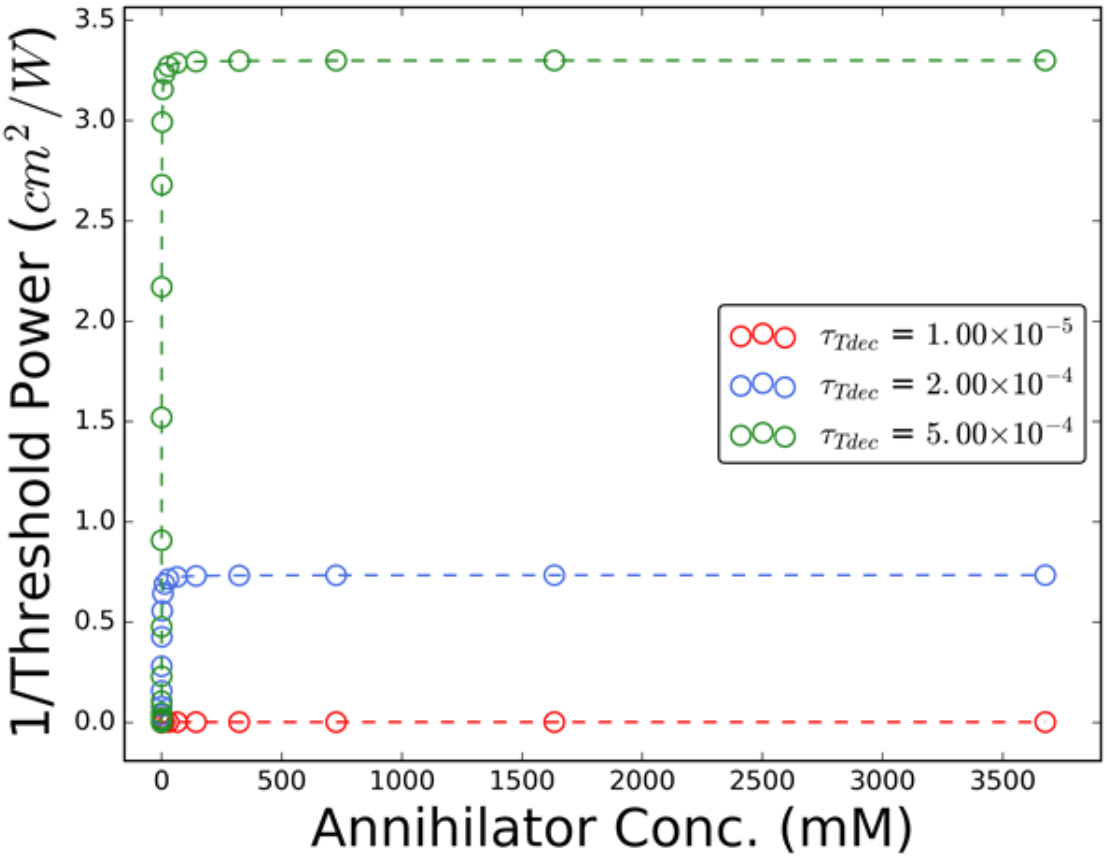

Figure S12. Simulated intensity threshold as a function of ground state annihilator concentration in solution showing the dependence of threshold intensity on τ_{Tdec}, the monomolecular decay lifetime of the triplet-excited state of the isolated annihilator molecule. As expected, a longer lifetime results in lower-power thresholds, as it allows triplet-excited annihilators greater opportunity to meet an annihilation partner and achieve upconversion.

These data show that annihilators with longer-lived triplet excited states can achieve efficient upconversion at a much lower threshold excitation intensity due to the kinetic competition between the monomolecular decay of triplet-excited annihilators and slow diffusion-mediated fusion interactions. However, again, this does not change the concentration of annihilators required for the lowest-achievable max-efficiency threshold.

Table S5. Kinetic parameters for Figure S12.

	Red	Green	Blue
k_{TF} (M^{-1} s^{-1})	1.00×10^{8}	1.00×10^{8}	1.00×10^{8}
k_{TET} (M^{-1} s^{-1})	1.00×10^{8}	1.00×10^{8}	1.00×10^{8}
τ_{Tdec} (s)	1.00×10^{-4}	2.00×10^{-4}	5.00×10^{-4}

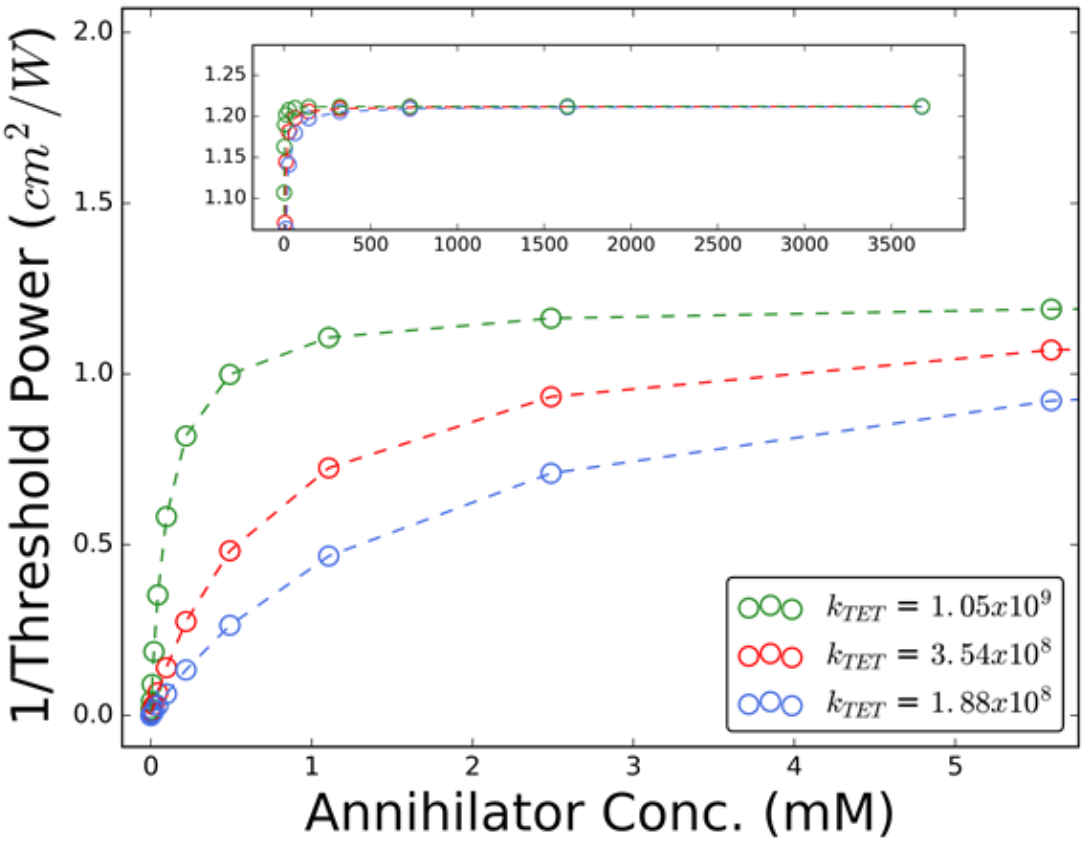

Figure S13. Simulated intensity threshold as a function of ground-state annihilator concentration in solution showing the dependence on k_{TET}, the rate constant for triplet transfer from sensitizer to annihilators, using the experimental values observed for our three annihilators from Stern-Volmer quenching. Inset: Alternate presentation of the data over a larger range of concentrations, showing that the k_{TET} does not affect the ultimate value of saturated intensity threshold, but instead influences the concentration of annihilators required for the lowest-achievable threshold.

In contrast to τ_{Tdec} and k_{TF}, k_{TET} clearly alters the functional form of the dependence of the threshold for max-efficiency upconversion on the annihilator concentration. This sets out the stark contrast between the model's accurate representation of the upconversion of the monomeric annihilators, and the inability to simultaneously capture the measured TET rates and UC photophysics for the dimeric annihilator.

Table S6. Kinetic parameters for Figure S13.

	Rubrene	TIPS-Tc	TIPS-BTc
k_{TF} (M^{-1} s^{-1})	1.00×10^8	1.00×10^8	1.00×10^8
k_{TET} (M^{-1} s^{-1})	3.54×10^8	1.05×10^9	1.88×10^8
τ_{Tdec} (s)	2.75×10^{-4}	2.75×10^{-4}	2.75×10^{-4}

Results of Kinetic Simulations: Concentration Dependence of UC Brightness

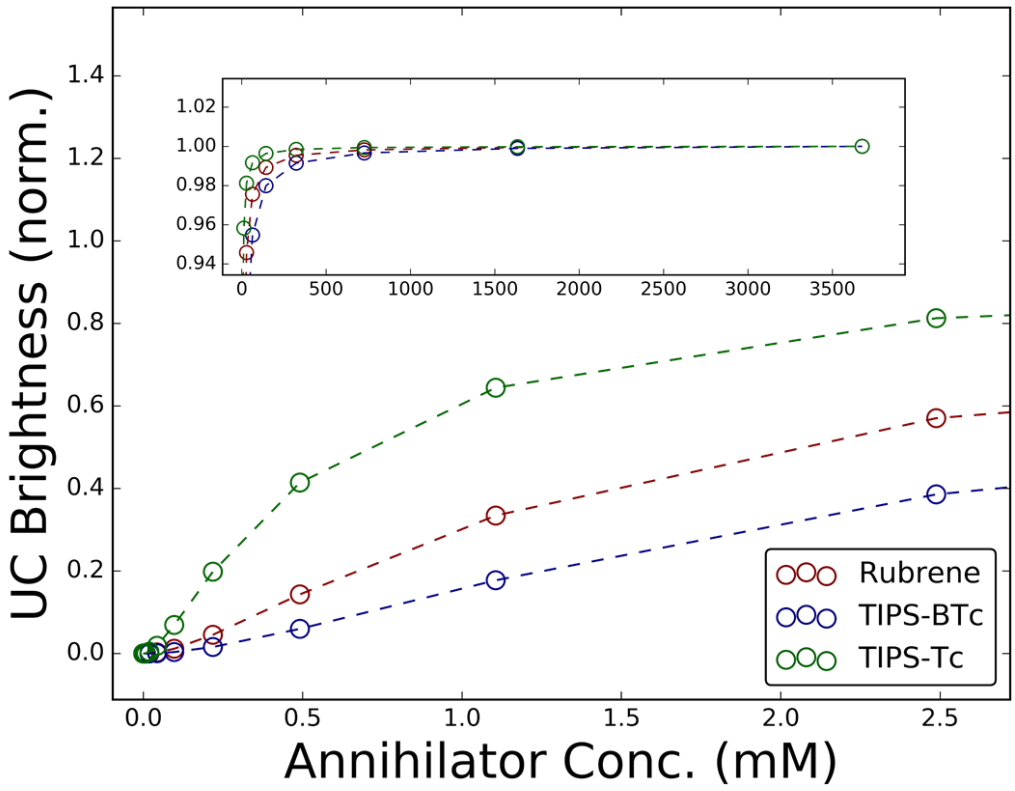

Figure 14. Simulated (normalized) UC brightness traces as a function of ground state annihilator concentration in solution, when excited above the threshold power for max efficiency upconversion. The TET rates considered for each annihilator are those extracted from Stern-Volmer quenching experiments Figure 2B, and the rates of TF are those considered for our best-fit parameters (Figure 2C). Inset: zoomed out presentation of the same simulation data, showing ultimate saturation of UC brightness.

Table S7. Kinetic parameters for Figure S14.

	Rubrene	TIPS-Tc	TIPS-BTc
k_{TF} (M^{-1} s^{-1})	7.14×10^{7}	1.11×10^{8}	1.00×10^{8}
k_{TET} (M^{-1} s^{-1})	3.54×10^{8}	1.05×10^{9}	1.88×10^{8}
τ_{dec} (s)	2.75×10^{-4}	2.75×10^{-4}	2.75×10^{-4}

Table S8. Kinetic parameters for Figure S10 and Figure 2C (main text).

	Rubrene	TIPS-Tc	TIPS-BTc	Unconstrained
k_{TF} (M^{-1} s^{-1})	7.14×10^{7}	1.11×10^{8}	1.00×10^{8}	1.00×10^{8}
k_{TET} (M^{-1} s^{-1})	3.54×10^{8}	1.05×10^{9}	1.88×10^{8}	1.00×10^{10}
τ_{Tdec} (s)	2.75×10^{-4}	2.75×10^{-4}	2.75×10^{-4}	2.75×10^{-4}

References

(1) Carey, T. J.; Snyder, J. L.; Miller, E. G.; Sammakia, T.; Damrauer, N. H. Synthesis of Geometrically Well-Defined Covalent Acene Dimers for Mechanistic Exploration of Singlet Fission. *The Journal of Organic Chemistry* **2017**, *82* (9), 4866–4874. https://doi.org/10.1021/acs.joc.7b00602.

(2) Cook, J. D.; Carey, T. J.; Arias, D. H.; Johnson, J. C.; Damrauer, N. H. Solvent-Controlled Branching of Localized versus Delocalized Singlet Exciton States and Equilibration with Charge Transfer in a Structurally Well-Defined Tetracene Dimer. *Journal of Physical Chemistry A* **2017**, *121* (48), 9229–9242. https://doi.org/10.1021/acs.jpca.7b09458.

(3) Gilligan, A. T.; Miller, E. G.; Sammakia, T.; Damrauer, N. H. Using Structurally Well-Defined Norbornyl-Bridged Acene Dimers to Map a Mechanistic Landscape for Correlated Triplet Formation in Singlet Fission. *Journal of the American Chemical Society* **2019**, *141* (14), 5961–5971. https://doi.org/10.1021/jacs.9b00904.

(4) Montalti, M.; Murov, S. L.; Carmichael, I.; Hug, G. L. *Handbook of Photochemistry*, 3rd ed.; CRC/Taylor & Francis: Boca Raton, Florida, USA, 1971.

(5) Zhou, J.; Liu, Q.; Feng, W.; Sun, Y.; Li, F. Upconversion Luminescent Materials: Advances and Applications. *Chemical Reviews* **2015**, *115* (1), 395–465. https://doi.org/10.1021/cr400478f.

(6) Haefele, A.; Blumhoff, J.; Khnayzer, R. S.; Castellano, F. N. Getting to the (Square) Root of the Problem: How to Make Noncoherent Pumped Upconversion Linear. *Journal of Physical Chemistry Letters* **2012**, *3* (3), 299–303. https://doi.org/10.1021/jz300012u.

(7) Bachilo, S. M.; Weisman, R. B. Determination of Triplet Quantum Yields from Triplet−Triplet Annihilation Fluorescence. *The Journal of Physical Chemistry A* **2000**, *104* (33), 7711–7714. https://doi.org/10.1021/jp001877n.

(8) Walker, B. J.; Musser, A. J.; Beljonne, D.; Friend, R. H. Singlet Exciton Fission in Solution. *Nature Chemistry* **2013**, *5* (12), 1019–1024. https://doi.org/10.1038/nchem.1801.

(9) Singh-Rachford, T. N.; Castellano, F. N. Photon Upconversion Based on Sensitized Triplet–Triplet Annihilation. *Coordination Chemistry Reviews* **2010**, *254* (21–22), 2560–2573. https://doi.org/10.1016/j.ccr.2010.01.003.

(10) Cheng, Y. Y.; Khoury, T.; Clady, R. G. C. R.; Tayebjee, M. J. Y.; Ekins-Daukes, N. J.; Crossley, M. J.; Schmidt, T. W. On the Efficiency Limit of Triplet–Triplet Annihilation for Photochemical Upconversion. *Phys. Chem. Chem. Phys.* **2010**, *12* (1), 66–71. https://doi.org/10.1039/B913243K.

(11) Cheng, Y. Y.; Fückel, B.; Khoury, T.; Clady, R. G. C. R.; Tayebjee, M. J. Y.; Ekins-Daukes, N. J.; Crossley, M. J.; Schmidt, T. W. Kinetic Analysis of Photochemical Upconversion by Triplet−Triplet Annihilation: Beyond Any Spin Statistical Limit. *The Journal of Physical Chemistry Letters* **2010**, *1* (12), 1795–1799. https://doi.org/10.1021/jz100566u.

(12) Scholes, G. D. Correlated Pair States Formed by Singlet Fission and Exciton–Exciton

Annihilation. *The Journal of Physical Chemistry A* **2015**, *119* (51), 12699–12705. https://doi.org/10.1021/acs.jpca.5b09725.

(13) Korovina, N. V.; Das, S.; Nett, Z.; Feng, X.; Joy, J.; Haiges, R.; Krylov, A. I.; Bradforth, S. E.; Thompson, M. E. Singlet Fission in a Covalently Linked Cofacial Alkynyltetracene Dimer. *Journal of the American Chemical Society* **2016**, *138* (2), 617–627. https://doi.org/10.1021/jacs.5b10550.

(14) Chen, M.; Krzyaniak, M. D.; Nelson, J. N.; Bae, Y. J.; Harvey, S. M.; Schaller, R. D.; Young, R. M.; Wasielewski, M. R. Quintet-Triplet Mixing Determines the Fate of the Multiexciton State Produced by Singlet Fission in a Terrylenediimide Dimer at Room Temperature. *Proceedings of the National Academy of Sciences* **2019**, *116* (17), 8178–8183. https://doi.org/10.1073/pnas.1820932116.

(15) Tayebjee, M. J. Y.; Sanders, S. N.; Kumarasamy, E.; Campos, L. M.; Sfeir, M. Y.; McCamey, D. R. Quintet Multiexciton Dynamics in Singlet Fission. *Nature Physics* **2017**, *13* (2), 182–188. https://doi.org/10.1038/nphys3909.

(16) Weiss, L. R.; Bayliss, S. L.; Kraffert, F.; Thorley, K. J.; Anthony, J. E.; Bittl, R.; Friend, R. H.; Rao, A.; Greenham, N. C.; Behrends, J. Strongly Exchange-Coupled Triplet Pairs in an Organic Semiconductor. *Nature Physics* **2017**, *13* (2), 176–181. https://doi.org/10.1038/nphys3908.

(17) Smith, M. B.; Michl, J. Singlet Fission. *Chemical Reviews* **2010**, *110* (11), 6891–6936. https://doi.org/10.1021/cr1002613.

(18) Eaves, J. D. Private Communications.

(19) Burdett, J. J.; Bardeen, C. J. Quantum Beats in Crystalline Tetracene Delayed Fluorescence Due to Triplet Pair Coherences Produced by Direct Singlet Fission. *Journal of the American Chemical Society* **2012**, *134* (20), 8597–8607. https://doi.org/10.1021/ja301683w.

(20) Rihter, B. D.; Kenney, M. E.; Ford, W. E.; Rodgers, M. A. J. Synthesis and Photoproperties of Diamagnetic Octabutoxyphthalocyanines with Deep Red Optical Absorbance. *Journal of the American Chemical Society* **1990**, *112* (22), 8064–8070. https://doi.org/10.1021/ja00178a032.